JOURNAL OF AIRCRAFT
Vol. 43, No. 5, September–October 2006

Dynamics of Corotating Vortex Filaments Part 1: Analytical Model

Teresa S. Miller,* Linda K. Kliment,* and Kamran Rokhsaz†
Wichita State University, Wichita, Kansas 67260-0044

DOI: 10.2514/1.22229

The interactions between two corotating vortex filaments of equal strength are investigated analytically. The Biot–Savart law is used to develop the equations of motion of the filaments, consistent with Crow's formulation. Consistent with previous work, two modes of motion are defined and analyzed for stability. It is demonstrated that the mutual induction between the vortices leads to unstable motion of the filaments in the antisymmetric mode over a significant range of frequencies. Furthermore, the oscillatory motion of the filaments is proven to have a preferred direction.

Nomenclature

a	=	core diameter
b_v	=	vortex separation distance
c	=	damping coefficient
d	=	integration cutoff distance
$d\boldsymbol{L}$	=	increment of length along the vortex
$\boldsymbol{e}_x, \boldsymbol{e}_y, \boldsymbol{e}_z$	=	unit vectors along x, y, and z
k	=	wave number
$\boldsymbol{R}$	=	general radial distance
$\boldsymbol{r}$	=	radial distance from mean vortex position
s	=	mean lateral vortex position
t	=	time
$\boldsymbol{U}_n$	=	induced velocity vector
u, v, w	=	perturbation velocity components
x, y, z	=	coordinate axes
$\hat{y}, \hat{z}$	=	perturbation amplitudes
α	=	dimensionless amplification rate, $=(2\pi b_v^2/\Gamma)c$
β	=	dimensionless wave number, $=kb_v$
Γ	=	vortex strength
δ	=	dimensionless cutoff distance, $=kd$
θ	=	inclination angle of the planes of motion
ξ	=	dimensionless length, $=\xi_n/b_v$
$\chi(\beta)$	=	first mutual-induction function, $=\int_0^\infty \cos(\beta\xi)/(\xi^2+1)^{3/2}\,\mathrm{d}\xi$
$\psi(\beta)$	=	second mutual-induction function, $=\int_0^\infty [\cos(\beta\xi)+\beta\xi\sin(\beta\xi)]/(\xi^2+1)^{3/2}\,\mathrm{d}\xi$
$\omega(\delta)$	=	self-induction function, $=\int_\delta^\infty [\cos(\xi)+\xi\sin(\xi)-1]/\xi^3\,\mathrm{d}\xi$

Subscripts

A	=	antisymmetric
S	=	symmetric
1, 2	=	left and right filaments

Introduction

THE vortical wake of an aircraft with deployed high-lift devices is a complex flowfield that has been the subject of numerous investigations. These flowfields are characterized by multiple corotating and counterrotating longitudinal vortex filaments. The kinematics of the counterrotating vortices have been studied extensively in analytical form [1,2] as well as experimentally [3–6]. However, one of the features of this flow in the near field is the interaction and the eventual merger of multiple corotating vortex filaments.

Considerable effort has been spent on studying the merger process from the viewpoint of viscosity and vortex diffusion. Two-dimensional models include those describing the visually observed phenomena [7] and analytical models of the merger process [8], verified experimentally [9]. Long-term behavior with real and simulated viscous effects has been shown to be sensitive to the initial conditions [10] and the background noise and turbulence [11,12]. There are also a number of papers addressing the stability of the motion of multiple inviscid vortices in two dimensions [13,14].

Three-dimensional investigations of corotating vortices have covered a wide range of topics as well. Detailed studies were made to understand the nature of the wake behind specific aircraft [15–18]. More recently, the distance to merger has been studied [19–21] and shown to be approximately one spiraling orbit, whereas more detailed studies have been made of the merger from the viewpoint of viscous diffusion [22].

All of the above investigations have focused on either the initial conditions or on the merger itself as a viscous phenomenon. The kinematics of the flow and the dynamic interactions between the corotating vortex filaments *before* merger have not received their due attention in the technical literature. Jimenez [23] offered the only analytical model that addresses this issue. However, his results did not agree entirely with the experimental results that have been obtained recently [24].

In the present paper, the authors report on their analytical investigation of the time-dependent interactions of a pair of corotating vortex filaments. An analytical approach similar to that of Crow [1] is used to investigate the stability of corotating vortex filaments. It is demonstrated that the filaments tend to form, in many cases, planer waves of increasing amplitude along preferred directions. The rate of growth of the amplitude and the inclination angles of the planes of motion are shown to depend on the wave number.

Method of Analysis

General Formulation

Figure 1 shows the schematic drawing of a pair of corotating vortex filaments and the associated coordinate system used for this analysis. Throughout this development, for the sake of clarity, the authors have adhered as closely as possible to the notation used by Crow [1].

The analysis begins with the Biot–Savart law, which relates the velocity and circulation in the following manner:

$$\boldsymbol{U}_n = \sum_{m=1}^{2} \Gamma_m \int_{-\infty}^{+\infty} \frac{\boldsymbol{R}_{mn} \times \mathrm{d}\boldsymbol{L}_m}{4\pi|\boldsymbol{R}_{mn}|^3} \tag{1}$$

Presented as Paper 2003-3601 at the AIAA 33rd Fluid Dynamics Conference and Exhibit, Orlando, FL, June 23–26, 2003; received 3 January 2006; revision received 3 January 2006; accepted for publication 6 January 2006.

*Graduate Research Assistant, Department of Aerospace Engineering. Student Member of AIAA

†Professor, Department of Aerospace Engineering. Associate Fellow of AIAA.

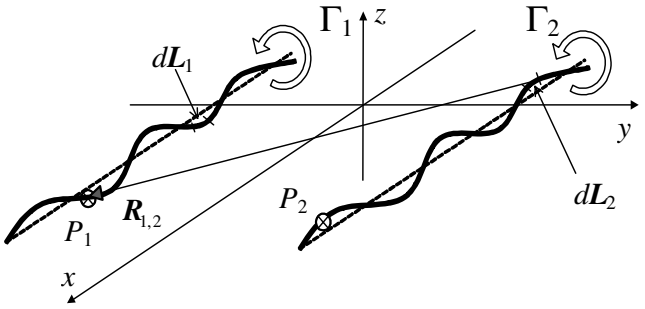

Fig. 1 Schematic of the geometry.

This equation gives the velocity vector induced at a point on vortex n by an element of length $\mathrm{d}\boldsymbol{L}$ on each of the two filaments. The position vector $\boldsymbol{R}_{mn}$ is defined as the vector from m to n and is given by

$$\boldsymbol{R}_{mn} = (x'_m - x_n)\boldsymbol{e}_x + (s_m - s_n)\boldsymbol{e}_y + (\boldsymbol{r}'_m - \boldsymbol{r}_n) \tag{2}$$

In the two vortex case, primes are used to distinguish points which lie on the same vortex, when $m = n$. The vector $\boldsymbol{r}$ lies in the y–z plane and denotes the vortex position relative to its mean location. Therefore,

$$\boldsymbol{r} = y(x,t)\boldsymbol{e}_y + z(x,t)\boldsymbol{e}_z \tag{3}$$

The line vortices have equal strength and rotate in the same direction so that $\Gamma = \Gamma_1 = \Gamma_2$. The associated boundary condition is the tangency of the local velocity vector to the filament, which translates into

$$\frac{\partial \boldsymbol{r}_n}{\partial x_n} u_n + \frac{\partial \boldsymbol{r}_n}{\partial t} = v_n \boldsymbol{e}_y + w_n \boldsymbol{e}_z \tag{4}$$

Furthermore, the differential length element directed along the vortex is given by

$$\mathrm{d}\,\boldsymbol{L}_m = \left[\boldsymbol{e}_x + \frac{\partial y'_m}{\partial x'_m}\boldsymbol{e}_y + \frac{\partial z'_m}{\partial x'_m}\boldsymbol{e}_z\right]\mathrm{d}x'_m \tag{5}$$

Substituting into Eq. (1) for the velocity $\boldsymbol{U}_n$ results in the following expressions for u_n, v_n, and w_n:

$$u_n = \sum_{m=1}^{2}\frac{\Gamma}{4\pi}\int_{-\infty}^{+\infty}\frac{1}{|\boldsymbol{R}_{mn}|^3}\left[(s_m - s_n)\frac{\partial z'_m}{\partial x'_m} + (y'_m - y_n)\frac{\partial z'_m}{\partial x'_m} - (z'_m - z_n)\frac{\partial y'_m}{\partial x'_m}\right]\mathrm{d}x'_m \tag{6}$$

$$v_n = \sum_{m=1}^{2}\frac{\Gamma}{4\pi}\int_{-\infty}^{+\infty}\frac{1}{|\boldsymbol{R}_{mn}|^3}\left[(z'_m - z_n) - (x'_m - x_n)\frac{\partial z'_m}{\partial x'_m}\right]\mathrm{d}x'_m \tag{7}$$

$$w_n = \sum_{m=1}^{2}\frac{\Gamma}{4\pi}\int_{-\infty}^{+\infty}\frac{1}{|\boldsymbol{R}_{mn}|^3}\left[(x'_m - x_n)\frac{\partial y'_m}{\partial x'_m} - (s_m - s_n) - (y'_m - y_n)\right]\mathrm{d}x'_m \tag{8}$$

where

$$|\boldsymbol{R}_{mn}|^{-3} = \{(x'_m - x_n)^2 + [(s_m - s_n) + (y'_m - y_n)]^2 + (z'_m - z_n)^2\}^{-3/2} \tag{9}$$

The integral equations can be linearized to the first order by a Taylor series expansion of Eq. (9), resulting in

$$|\boldsymbol{R}_{mn}|^{-3} \approx \frac{1}{[(x'_m - x_n)^2 + (s_m - s_n)^2]^{3/2}} - \frac{3(s_m - s_n)(y'_m - y_n)}{[(x'_m - x_n)^2 + (s_m - s_n)^2]^{5/2}} \tag{10}$$

Substituting Eq. (10) into Eqs. (6–8) and eliminating the second and higher order terms leads to

$$u_n = \sum_{m=1}^{2}\frac{\Gamma}{4\pi}\int_{-\infty}^{\infty}\frac{(s_m - s_n)\frac{\partial z'_m}{\partial x'_m}}{[(x'_m - x_n)^2 + (s_m - s_n)^2]^{3/2}}\,\mathrm{d}x'_m \tag{11}$$

$$v_n = \sum_{m=1}^{2}\frac{\Gamma}{4\pi}\int_{-\infty}^{\infty}\frac{(z'_m - z_n) - (x'_m - x_n)\frac{\partial z'_m}{\partial x'_m}}{[(x'_m - x_n)^2 + (s_m - s_n)^2]^{3/2}}\,\mathrm{d}x'_m \tag{12}$$

$$w_n = \sum_{m=1}^{2}\frac{\Gamma}{4\pi}\left[\int_{-\infty}^{\infty}\frac{(x'_m - x_n)\frac{\partial y'_m}{\partial x'_m} - (y'_m - y_n)}{[(x'_m - x_n)^2 + (s_m - s_n)^2]^{3/2}}\,\mathrm{d}x'_m + \int_{-\infty}^{\infty}\frac{3(s_m - s_n)^2(y'_m - y_n)}{[(x'_m - x_n)^2 + (s_m - s_n)^2]^{5/2}}\,\mathrm{d}x'_m - \int_{-\infty}^{\infty}\frac{(s_m - s_n)}{[(x'_m - x_n)^2 + (s_m - s_n)^2]^{3/2}}\,\mathrm{d}x'_m\right] \tag{13}$$

The position of the unperturbed vortex along the y axis is given by the variable s that is defined as one-half the distance between the two vortices where $s_1 = -b_v/2$ and $s_2 = +b_v/2$. Therefore, the last integral on the right-hand side of Eq. (13) becomes

$$\sum_{m=1}^{2}\frac{\Gamma}{4\pi}\int_{-\infty}^{\infty}\frac{(s_m - s_n)}{[(x'_m - x_n)^2 + (s_m - s_n)^2]^{3/2}}\,\mathrm{d}x'_m = \sum_{m=1}^{2}\frac{\Gamma}{4\pi}\left(\frac{2}{s_m - s_n}\right) \tag{14}$$

For the first vortex, $m = 1$, this term is

$$\frac{\Gamma}{4\pi}\left(\frac{2}{s_1 - s_2}\right) = \frac{-\Gamma}{2\pi b_v} \tag{15}$$

and for the second vortex, $m = 2$, this term is

$$\frac{\Gamma}{4\pi}\left(\frac{2}{s_2 - s_1}\right) = \frac{\Gamma}{2\pi b_v} \tag{16}$$

These terms are time independent and indicate that the two vortices spiral around each other about the x axis at a constant rate. These terms, being constants, have no contribution in the ensuing stability analysis. Therefore, they will be ignored in the remainder of this work. This is the same as assuming that the coordinate system rotates around the x axis at a constant rate determined by the induced velocities from these terms.

The first term on the left-hand side of Eq. (4) is a higher order term and is therefore neglected. Substituting the perturbation velocities in the remaining terms results in

$$\frac{\partial \boldsymbol{r}_n}{\partial t} = \sum_{m=1}^{2}\frac{\Gamma}{4\pi}\left\{\left[\int_{-\infty}^{\infty}\frac{(z'_m - z_n) - (x'_m - x_n)\frac{\partial z'_m}{\partial x'_m}}{[(x'_m - x_n)^2 + (s_m - s_n)^2]^{3/2}}\,\mathrm{d}x'_m\right]\boldsymbol{e}_y + \left[\int_{-\infty}^{\infty}\frac{(x'_m - x_n)\frac{\partial y'_m}{\partial x'_m} - (y'_m - y_n)}{[(x'_m - x_n)^2 + (s_m - s_n)^2]^{3/2}} + \frac{3(s_m - s_n)^2(y'_m - y_n)}{[(x'_m - x_n)^2 + (s_m - s_n)^2]^{5/2}}\,\mathrm{d}x'_m\right]\boldsymbol{e}_z\right\} \tag{17}$$

Stability Analysis

For an exponential stability analysis, one can assume perturbations of the form

$$\boldsymbol{r}_n = \hat{y}_n e^{ct + ikx_n}\boldsymbol{e}_y + \hat{z}_n e^{ct + ikx_n}\boldsymbol{e}_z \tag{18}$$

In this case, Eq. (17) leads to two sets of equations, each having two parts: a projection on the x–y plane and a projection on the x–z plane. The case of $n = 1$ will be considered here. The case of $n = 2$ follows the same steps.

The projection on the x–y plane is given by

$$c\hat{y}_1 = \frac{\Gamma}{4\pi}\hat{z}_1\int_{-\infty}^{\infty}\frac{(e^{ik\xi_1}-1)-ik\xi_1 e^{ik\xi_1}}{|\xi_1|^3}\,\mathrm{d}\xi_1 + \frac{\Gamma}{4\pi}\int_{-\infty}^{\infty}\frac{(\hat{z}_2 e^{ik\xi_2}-\hat{z}_1)-ik\xi_2\hat{z}_2 e^{ik\xi_2}}{[\xi_2^2+b_v^2]^{3/2}}\,\mathrm{d}\xi_2 \tag{19}$$

where

$$\xi_1 = x_1' - x_1 \tag{20}$$

and

$$\xi_2 = x_2' - x_1 \tag{21}$$

Using the following substitution for the exponential terms

$$e^{ik\xi_n} = \cos(k\xi_n) + i\sin(k\xi_n) \tag{22}$$

Equation (19) becomes

$$\begin{aligned} c\hat{y}_1 = {} & \frac{\Gamma}{4\pi}\hat{z}_1\int_{-\infty}^{\infty}\left[\frac{\cos(k\xi_1)+k\xi_1\sin(k\xi_1)-1}{|\xi_1|^3} + \frac{i[\sin(k\xi_1)-k\xi_1\cos(k\xi_1)]}{|\xi_1|^3}\right]\mathrm{d}\xi_1 \\ & + \frac{\Gamma}{4\pi}\hat{z}_2\int_{-\infty}^{\infty}\left[\frac{\cos(k\xi_2)+k\xi_2\sin(k\xi_2)}{(\xi_2^2+b_v^2)^{3/2}} + \frac{i[\sin(k\xi_2)-k\xi_2\cos(k\xi_2)]}{(\xi_2^2+b_v^2)^{3/2}}\right]\mathrm{d}\xi_2 \\ & - \frac{\Gamma}{4\pi}\hat{z}_1\int_{-\infty}^{\infty}\left[\frac{1}{(\xi_2^2+b_v^2)^{3/2}}\right]\mathrm{d}\xi_2 \end{aligned} \tag{23}$$

The real parts of the integrals in Eq. (23) are even functions, whereas the imaginary parts are odd. Therefore, integrating over the infinite domain results in a finite value for the real parts, but the integrals of the imaginary parts vanish. Furthermore, the integrals contain a strong singularity where $\xi_1 = 0$. To remove this singularity, a small part of the domain is ignored in the integration process by introducing a small cutoff distance. Ignoring the contribution of the imaginary parts and incorporating the cutoff distance d in the self-induction term yields

$$c\hat{y}_1 = \frac{\Gamma}{2\pi}\hat{z}_1\int_{d}^{\infty}\frac{\cos(k\xi_1)+k\xi_1\sin(k\xi_1)-1}{\xi_1^3}\,\mathrm{d}\xi_1 + \frac{\Gamma}{2\pi}\hat{z}_2\int_{0}^{\infty}\frac{\cos(k\xi_2)+k\xi_2\sin(k\xi_2)}{(\xi_2^2+b_v^2)^{3/2}}\,\mathrm{d}\xi_2 - \frac{\Gamma}{2\pi b_v^2}\hat{z}_1 \tag{24}$$

Similarly, one can show that for the projection on the x–z plane

$$c\hat{z}_1 = \frac{-\Gamma}{2\pi}\hat{y}_1\int_{d}^{\infty}\frac{\cos(k\xi_1)+k\xi_1\sin(k\xi_1)-1}{\xi_1^3}\,\mathrm{d}\xi_1 + \frac{\Gamma}{2\pi}\hat{y}_2\int_{0}^{\infty}\frac{\cos(k\xi_2)}{(\xi_2^2+b_v^2)^{3/2}}\,\mathrm{d}\xi_2 - \frac{\Gamma}{2\pi b_v^2}\hat{y}_1 \tag{25}$$

Equations (24) and (25) can be rewritten in terms of the dimensionless variables as follows:

$$\alpha\hat{y}_1 = \beta^2\hat{z}_1\int_{\delta}^{\infty}\frac{\cos(\beta\xi)+\beta\xi\sin(\beta\xi)-1}{(\beta\xi)^3}\,\mathrm{d}(\beta\xi) + \hat{z}_2\int_{0}^{\infty}\frac{\cos(\beta\xi)+\beta\xi\sin(\beta\xi)}{(\xi^2+1)^{3/2}}\,\mathrm{d}\xi - \hat{z}_1 \tag{26}$$

$$\alpha\hat{z}_1 = -\beta^2\hat{y}_1\int_{\delta}^{\infty}\frac{\cos(\beta\xi)+\beta\xi\sin(\beta\xi)-1}{(\beta\xi)^3}\,\mathrm{d}(\beta\xi) + \hat{y}_2\int_{0}^{\infty}\frac{\cos(\beta\xi)}{(\xi^2+1)^{3/2}}\,\mathrm{d}\xi - \hat{y}_1 \tag{27}$$

or simply

$$\alpha\hat{y}_1 = \beta^2\omega\hat{z}_1 + \psi\hat{z}_2 - \hat{z}_1 \tag{28}$$

$$\alpha\hat{z}_1 = -\beta^2\omega\hat{y}_1 + \chi\hat{y}_2 - \hat{y}_1 \tag{29}$$

Following the same procedure for $n = 2$ produces

$$\alpha\hat{y}_2 = \beta^2\omega\hat{z}_2 + \psi\hat{z}_1 - \hat{z}_2 \tag{30}$$

$$\alpha\hat{z}_2 = -\beta^2\omega\hat{y}_2 + \chi\hat{y}_1 - \hat{y}_2 \tag{31}$$

Therefore, to determine the eigenvalues and the eigenvectors, one must solve the linear system given by Eqs. (28–31).

The symmetric and the antisymmetric solutions are considered separately by Crow [1] and by Jimenez [23]. For the corotating case, these modes are defined as

$$\hat{y}_A = \hat{y}_2 - \hat{y}_1 \tag{32}$$

$$\hat{z}_A = \hat{z}_2 - \hat{z}_1 \tag{33}$$

$$\hat{y}_S = \hat{y}_2 + \hat{y}_1 \tag{34}$$

$$\hat{z}_S = \hat{z}_2 + \hat{z}_1 \tag{35}$$

Jimenez [23] indicates that the antisymmetric mode consists of the oscillations of the two vortex filaments as a whole, whereas the symmetric mode describes the internal perturbations of the system. The roots for the symmetric mode are given by

$$\alpha_S^2 = (\beta^2\omega + \psi - 1)(-\beta^2\omega + \chi - 1) \tag{36}$$

The roots for the antisymmetric mode are given by

$$\alpha_A^2 = (\beta^2\omega - \psi - 1)(-\beta^2\omega - \chi - 1) \tag{37}$$

To investigate the stability of the system, the amplification rates found in Eq. (36) and (37) must be analyzed. Crow [1] shows the following to be true:

$$\chi(\beta) = \beta K_1(\beta) \tag{38}$$

$$\psi(\beta) = \beta^2 K_0(\beta) + \beta K_1(\beta) \tag{39}$$

$$\omega(\delta) = \frac{1}{2}\left[\frac{\cos\delta - 1}{\delta^2} + \frac{\sin\delta}{\delta} - Ci(\delta)\right] \tag{40}$$

where $Ci(\delta)$ is the cosine integral and K_n are modified Bessel functions. Figure 2 shows the mutual-induction functions ψ and χ

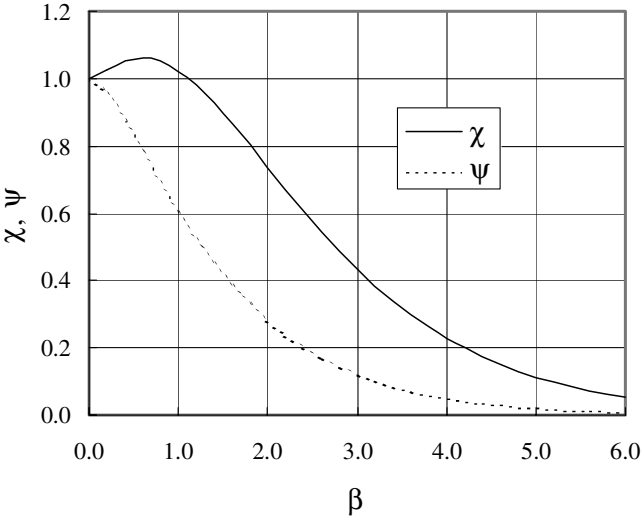

Fig. 2 Mutual-induction functions.

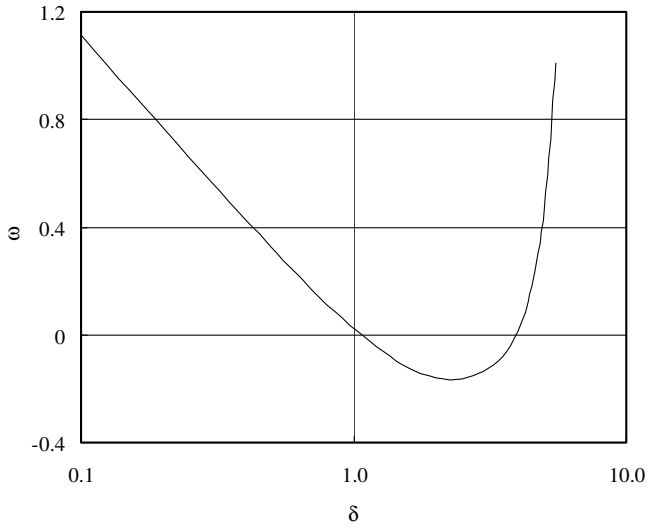

Fig. 3 Self-induction function.

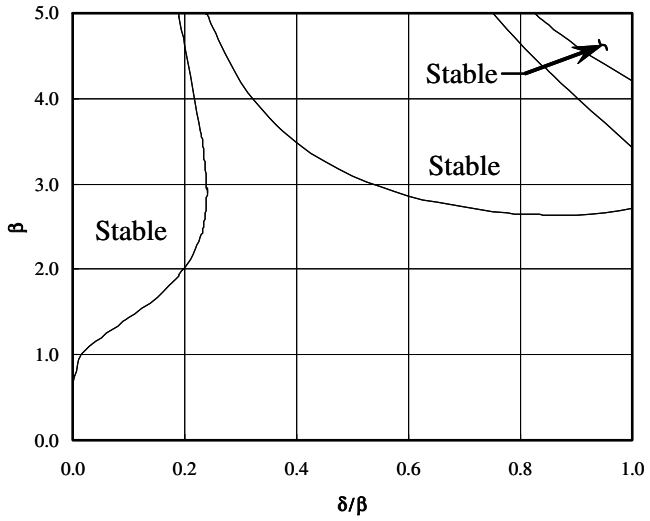

Fig. 4 Stability diagram for the antisymmetric mode.

versus the dimensionless wave number, and Fig. 3 shows the self-induction term ω as a function of the dimensionless cutoff distance.

For both the symmetric and antisymmetric cases, the mode is unstable when the value of α^2, given by Eqs. (36) and (37), is positive. When α^2 is negative, the mode is neutrally stable. Crow [1] characterizes this behavior as similar to the oscillations of a single vortex. He also states that the vortices are twisted into traveling helices or have motion confined to spinning planes. Figure 4 is the stability diagram for the antisymmetric mode, and Fig. 5 is the stability diagram for the symmetric mode. It can be seen from these diagrams that the corotating case has both stable and unstable regions. This is in contrast to the results obtained by Jimenez [23] who found the motion of the corotating vortices to be stable over a wide range of frequencies. Variations of α^2 as a function of β for three values of the nondimensional cutoff distance are shown in Figs. 6–8.

Crow [1] showed that, for the unstable counterrotating vortices, the growing perturbations are planar standing waves. He described the planes at fixed angles $\theta(\beta, \delta)$ relative to the horizontal. For the corotating case, angle θ is defined relative to the line connecting the mean vortex positions and is given by

$$\tan\theta = \frac{\hat{z}}{\hat{y}} \tag{41}$$

Therefore, for the symmetric mode

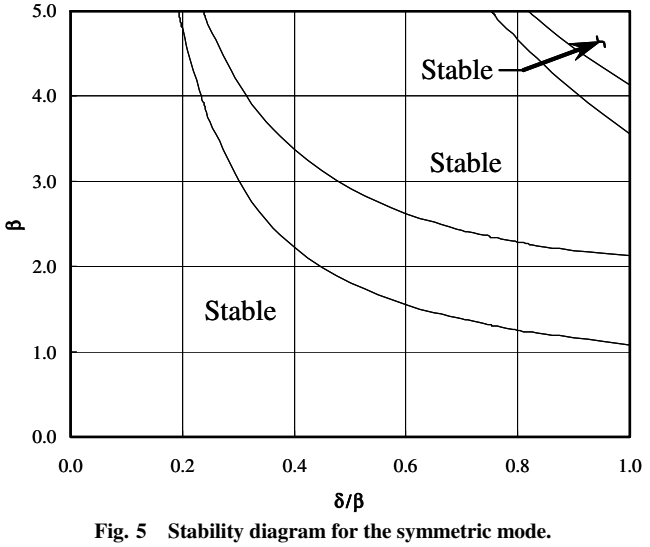

Fig. 5 Stability diagram for the symmetric mode.

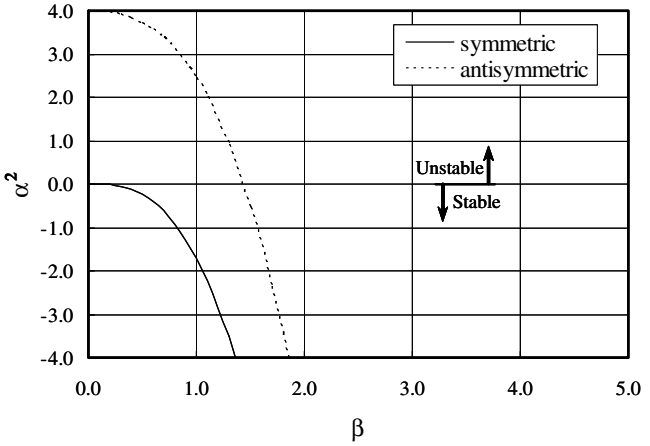

Fig. 6 Profile plot of $\delta/\beta = 0.10$.

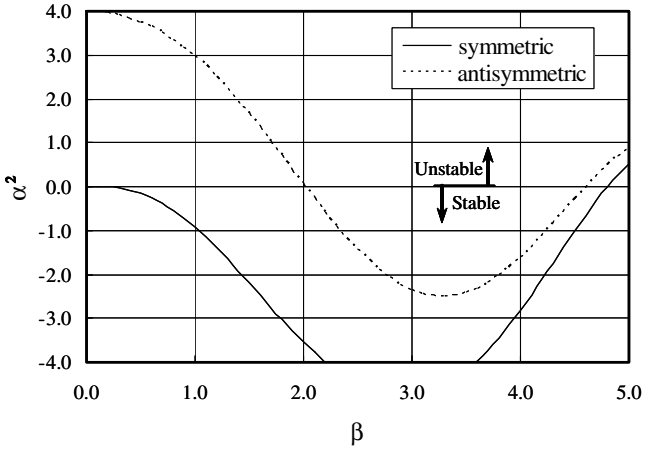

Fig. 7 Profile plot of $\delta/\beta = 0.20$.

$$\tan^2\theta_S = \frac{(-\beta^2\omega + \chi - 1)}{(\beta^2\omega + \psi - 1)} \tag{42}$$

and for the antisymmetric mode

$$\tan^2\theta_A = \frac{(-\beta^2\omega - \chi - 1)}{(\beta^2\omega - \psi - 1)} \tag{43}$$

The angles for both modes are shown graphically in Figs. 9 and 10.

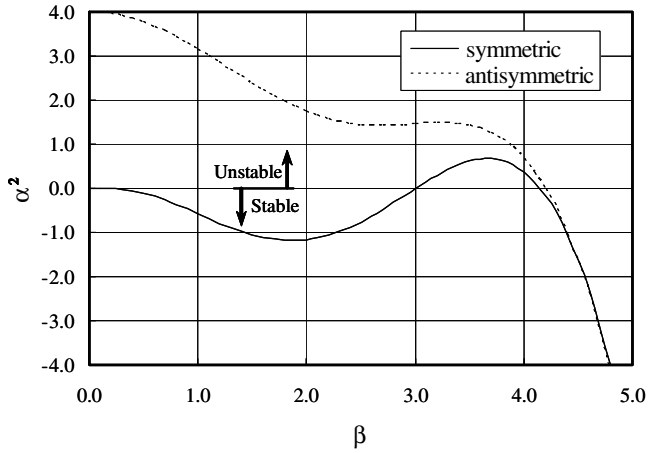

Fig. 8 Profile plot of $\delta/\beta = 0.30$.

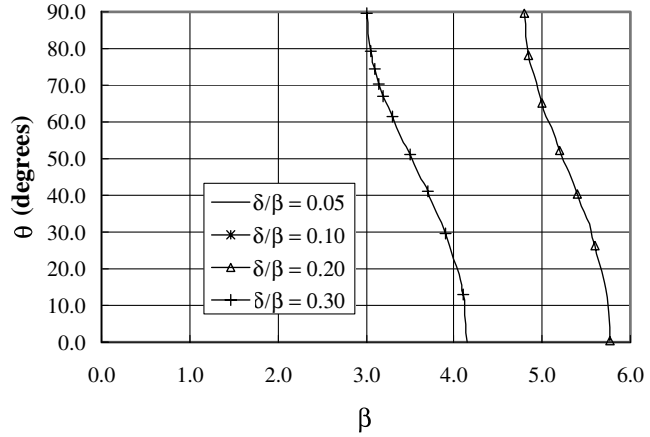

Fig. 9 Angles of planar standing waves for the symmetric mode.

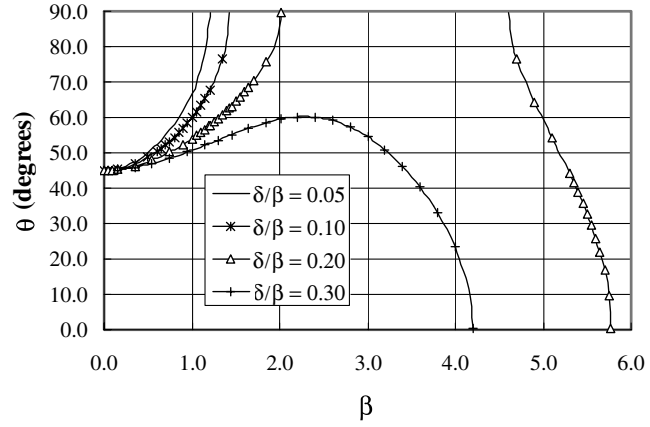

Fig. 10 Angles of planar standing waves for the antisymmetric mode.

From the previous discussion, it is clear that the results of this analysis are in contrast to those of Jimenez [23]. Currently, there is a limited amount of data available in the literature that tends to support the present conclusions [24,25]. However, a conclusive set of experimental data that would support this analysis is lacking.

Conclusions

An analytical model for the interactions between corotating longitudinal vortices was developed. The vortices were assumed to be of equal strength. This model, which relied on the Biot–Savart law, was shown to be consistent with those of Jimenez and Crow. Consistent with other models, two modes of motion were defined to describe the movements of filaments relative to each other. In the symmetric mode, the filaments would move relative to each other, whereas the antisymmetric mode described the motion of the system as a whole.

It was proven analytically that the mutual induction between the vortices would lead to unstable motion of the filaments over a wide range of frequencies in the antisymmetric mode. Also, the oscillatory motion of the filaments was proven to have a preferred direction.

The outcomes shown here are inconsistent with the widely accepted results of Jimenez. Therefore, further experimental investigation of the role of the frequency is recommended.

Appendix

Examining the analysis presented by Jimenez [23] in more detail, he defines the following variables:

$$M(\beta) = \tfrac{1}{2}\beta^2 K_2(\beta) \tag{A1}$$

$$Q(\beta) = \beta K_1(\beta) + \beta^2 K_0(\beta) \tag{A2}$$

$$\Omega = \tfrac{1}{2}\beta^2[1.059 - \ell_n(\beta a/b_v)] \tag{A3}$$

Following the method described by Jimenez but transforming into the coordinate system used for the current analysis, the basic modes of the first vortex are defined as

$$\alpha_J \hat{y}_1 = \tfrac{1}{2}(1+\Omega)\hat{z}_1 + \tfrac{1}{2}Q\hat{z}_2 \tag{A4}$$

$$\alpha_J \hat{z}_1 = -\tfrac{1}{2}(3+\Omega)\hat{y}_1 - (\tfrac{1}{2}Q - M)\hat{y}_2 \tag{A5}$$

whereas for the second vortex the results are

$$\alpha_J \hat{y}_2 = +\tfrac{1}{2}Q\hat{z}_1 + \tfrac{1}{2}(1+\Omega)\hat{z}_2 \tag{A6}$$

$$\alpha_J \hat{z}_2 = -(\tfrac{1}{2}Q - M)\hat{y}_1 - \tfrac{1}{2}(3+\Omega)\hat{y}_2 \tag{A7}$$

The subscript J is used here to distinguish between the basic modes identified by Jimenez and the basic modes developed in the present analysis that have no subscript and are given in Eqs. (28–31). The modes given by Jimenez are clearly different from those found in the current analysis.

References

[1] Crow, S. C., "Stability Theory for a Pair of Trailing Vortices," *AIAA Journal*, Vol. 8, No. 12, Dec. 1970, pp. 2172–2179.

[2] Crouch, J. D., "Instability and Transient Growth for Two Trailing-Vortex Pairs," *Journal of Fluid Mechanics*, Vol. 350, Nov. 1997, pp. 311–330.

[3] Eliason, B. G., Gartshere, I. S., and Parkinson, G. V., "Wind Tunnel Investigation of Crow Instability," *Journal of Aircraft*, Vol. 12, No. 12, Dec. 1975, pp. 985–988.

[4] Rebours, R., "Quantitative Measurement of Wake Vortex Motion in a Water Tunnel," M.S. Thesis, Wichita State University, Wichita, KS, May 2001.

[5] Rossow, V. J., "Prospects for Destructive Self-Induced Interactions in a Vortex Pair," *Journal of Aircraft*, Vol. 24, No. 7, July 1987, pp. 433–440.

[6] Rebours, R., and Rokhsaz, K., "Flap Sizing for Wake Vortex Instability," Society of Automotive Engineers Paper SAE-2000-01-1693, 2000.

[7] Greene, G. C., "An Approximate Model of Vortex Decay in the Atmosphere," *Journal of Aircraft*, Vol. 23, No. 7, July 1986, pp. 566–573.

[8] Saffman, P. G., *Vortex Dynamics*, Cambridge Univ. Press, New York, 1997.

[9] Meunier, P., and Leweke, T., "Merging and Three-Dimensional Instability of a Corotating Vortex Pair," *Vortex Structure and Dynamics: Lectures of a Workshop Held in Rouen, France*, edited by A. Maurel, and P. Petitjeans, Springer–Verlag, Berlin, 2000, pp. 241–251.

[10] Rossow, V. J. "Convective Merging of Vortex Cores in Lift-Generated Wakes," *Journal of Aircraft*, Vol. 14, No. 3, March 1977, pp. 283–290.

[11] Caperan, P., and Verron, J., "Numerical Simulation of a Physical Experiment on Two-Dimensional Vortex Merging," *Fluid Dynamics Research*, Vol. 3, No. 1–4, Sept. 1988, pp. 87–92.
[12] Basu, A. J., "The Role of Noise in Two-Dimensional Vortex Merging," *Fluid Dynamics Research*, Vol. 10, No. 3, Nov. 1992, pp. 169–180.
[13] Hassan, A., "Motion of Three Vortices," *Physics of Fluids*, Vol. 22, No. 3, March 1979, pp. 393–400.
[14] Eckhardt, B., "Integrable Four Vortex Motion," *Physics of Fluids*, Vol. 31, No. 10, Oct. 1988, pp. 2796–2801.
[15] Dunham, R. E., Jr., "Model Tests of Various Vortex Dissipation Techniques in a Water Towing Tank," NASA LWP-1146, Jan. 1974.
[16] Corsiglia, V. R., and Dunham, R. E., Jr., "Aircraft Wake Vortex Minimization by Use of Flaps," *NASA Symposium on Wake Vortex Minimization*, SP-409, NASA, 1976, pp. 303–336.
[17] Corsiglia, V. R., Rossow, V. J., and Ciffone, D. L., "Experimental Study of the Effect of Span Loading on Aircraft Wakes," *Journal of Aircraft*, Vol. 13, No. 12, Dec. 1976, pp. 968–973.
[18] Tymczyszyn, J. J., and Barber, M. R., "Recent Wake Turbulence Flight Test Programs," *Aerospace Profession–Eighteenth Symposium Proceedings*, Society of Experimental Test Pilots, Lancaster, CA, Sept. 1974, pp. 52–68.
[19] Jacob, J. D., "Experimental Investigation of Co-Rotating Trailing Vortices," AIAA Paper 1998-0590, 1998.
[20] Jacob, J. D., "Experiments on Trailing Vortex Merger," AIAA Paper 1999-0547, 1999.
[21] Jacob, J. D., and Savas, O., "Vortex Dynamics in Trailing Wakes of Flapped Rectangular Wings," AIAA Paper 1997-0048, 1997.
[22] Cerretelli, C., and Williamson, C. H. K., "The Physical Mechanism for Vortex Merging," *Journal of Fluid Mechanics*, Vol. 475, Jan. 2003, pp. 41–77.
[23] Jimenez, J., "Stability of a Pair of Co-Rotating Vortices," *Physics of Fluids*, Vol. 18, No. 11, Nov. 1975, pp. 1580–1581.
[24] Kliment, L. K., "Experimental Investigation of Flap Tip and Wing Tip Vortex Interactions," M.S. Thesis, Wichita State University, Wichita, KS, Dec. 2002.
[25] Rokhsaz, K., and Kliment, L. K., "Experimental Investigation of Co-Rotating Vortex Filaments in a Water Tunnel," AIAA Paper 2002-3303, 2002.